ROZPRAWY INŻYNIERSKIE • ENGINEERING TRANSACTIONS • 27, 4, 633—649, 1979
Polska Akademia Nauk • Instytut Podstawowych Problemów Techniki

THE STABILITY AND POST-BUCKLING STATE OF A RECTANGULAR DISK UNDER UNIDIRECTIONAL BENDING AND SIMULTANEOUS SHEAR

W. WALCZAK and S. JAKUBOWSKI (ŁÓDŹ)

The problem stated in the title concerns an isotropic, rectangular disk, simply supported along its edges. In order to obtain an approximate solution of the problem, the deflection function $w(x,y)$ describing the middle surface of the disk after stability loss is assumed in the form of the series which satisfy the boundary conditions of the problem. The Airy's stress function $\Phi(x,y)$ was also introduced.

To determine these functions, the Kármán differential equations of the nonlinear theory of plates were used. The parameters in the deflection function $w(x,y)$ were determined by means of the Bubnov-Galerkin method.

As a result of this, equations from which the stress and strain components could be determined by dimensionless coefficients were obtained. These equations were then used for detailed computations of the disk for which the ratio of the edge lengths $\lambda=a/b=0.9$.

The results of computations were presented in the form of graphs prepared in a form useful for practical calculations.

1. Introduction

Thin-walled rectangular disks as the principal load-carrying elements of sheet-iron girder constructions, usually work in conditions of complex state of loading.

From the point of view of practical engineering applications, the case of unidirectional disk bending and simultaneous shear is espacially important. This case of loading occurs in almost each load-carrying construction.

The number of papers devoted to investigations of the stability and post-buckling state of rectangular disks under simultaneous bending and shear is relatively small. In this domain I. I. Aare's and S. I. Indurms papers [5] and [6] deserve particular attention.

However, a more detailed analysis of disk behaviour in the post-buckling state cannot be carried out on the basis of these papers. The latter mainly present the results of numerical computations. This is why there is still a need for more extensive discussion and explanations.

In this situation it seems purposeful and necessary to analyse more closely the stability and post-buckling behaviour of a rectangular disk under the loading conditions mentioned in the title.

2. Assumption and governing differential equations

The subject under consideration is a thin, rectangular, isotropic disk of dimensions $a \times b$ and a constant thickness h, simply supported along its perimeter. It is assumed that the edges of the disk are reinforced by suitable ribs stiff enough to maintain the rectilinearity of these edges. A Cartesian coordinate system x, y, z (Fig. 1) is assumed.

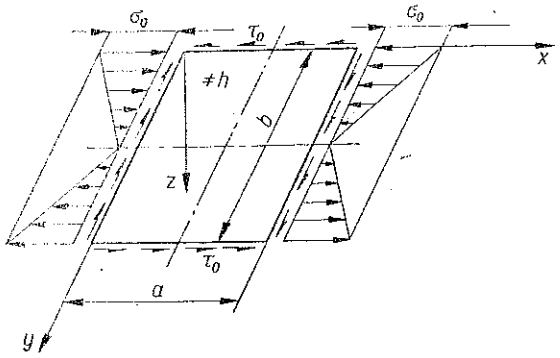

Fig. 1. Scheme of the disk loading.

All the disk edges are subjected to the action of uniformly distributed shear stresses of a constant value τ_0 and, moreover, the edges $x=0$ and $x=a$ (Fig. 1) are additionally loaded by normal stresses σ. The loads are applied in the middle surface of the disk.

The distribution of normal stresses σ along the mentioned edges is expressed by the following formula:

$$\sigma=\sigma_0\left(1-\alpha\frac{y}{b}\right), \tag{2.1}$$

σ_0 being the maximum value of σ. For the coefficient α the value $\alpha=2$ is taken. It corresponds to the case of pure disk bending. It is assumed that the loading parameters σ_0 and τ_0 may reach values exceeding the critical values.

The problem was solved on the basis of the nonlinear theory of plates. This theory provides the two governing nonlinear, partial differential equations beeing called Kármán's equations [3]:

$$\frac{D}{h}\nabla^2\nabla^2(w)-L(w,\Phi)=0 \tag{2.2}$$

and

$$\frac{1}{E}\nabla^2\nabla^2(\Phi)+\frac{1}{2}L(w,w)=0, \tag{2.3}$$

where E — Young's modulus, $D=\dfrac{Eh^3}{12(1-\nu^2)}$ — flexural rigidity of a disk, ν — Poisson's ratio. These equations contain two unknown functions: the Airy's stress

function $\Phi=\Phi(x, y)$ and the deflection function $w=w(x, y)$ describing the shape of the middle surface of a disk after buckling. The symbol $L(w, \Phi)$ refers to the nonlinear differential operator defined as follows:

$$L(w, \Phi)=\frac{\partial^2 w}{\partial x^2}\frac{\partial^2 \Phi}{\partial y^2}+\frac{\partial^2 w}{\partial y^2}\frac{\partial^2 \Phi}{\partial x^2}-2\frac{\partial^2 w}{\partial x\,\partial y}\frac{\partial^2 \Phi}{\partial x\,\partial y}. \tag{2.4}$$

A solution of the system of equations (2.2) and (2.3) which may be obtained only by approximate methods enables to determine the stress function $\Phi(x, y)$ and the deflection function $w(x, y)$. A knowledge of these functions makes it possible to determine all parameters of the strain and stress states of the considered disk after buckling. Then, with the aid of the stress function $\Phi(x, y)$ we can determine all the components of the membrane stress state and, by means of the deflection function $w(x, y)$, all the components of the bending state. This makes it possible to carry out an analysis of the critical and post-buckling states.

3. Solution of the problem

In order to obtain an approximate solution of the problem mentioned in the title, the normal deflection w of the disk was defined by a function describing as closely as possible the shape of the middle surface of the disk after buckling. On the basis of the result of [3, 4, 5 and 7], the function $w(x, y)$ is assumed as follows:

$$w(x, y)=f_{11}\sin\frac{\pi x}{a}\sin\frac{\pi y}{b}+f_{22}\sin\frac{2\pi x}{a}\sin\frac{2\pi y}{b}+f_{12}\sin\frac{\pi x}{a}\sin\frac{2\pi y}{b}, \tag{3.1}$$

where f_{11}, f_{22} and f_{12} are unknown coefficients of the normal disk deflection. This function fulfils the boundary conditions of a simple support of the disk edges.

Equation (2.3) is used to determine an approximate form of the Airy's stress function $\Phi(x, y)$. The general solution of this equation with $w(x, y)$ given by Eq. (3.1) has the following form:

$$\begin{aligned}\Phi(x, y)=\frac{E}{4\lambda^2}\Bigg\{&-f_{11}f_{12}\cos\frac{\pi y}{b}+\frac{f_{11}^2}{8}\cos\frac{2\pi y}{b}+\frac{f_{11}f_{12}}{9}\cos\frac{3\pi y}{b}+\\&+\frac{4f_{22}^2+f_{12}^2}{32}\cos\frac{4\pi y}{b}+4\lambda^4 f_{22}\Bigg[-f_{12}+\frac{4f_{11}}{(1+9\lambda^2)^2}\cos\frac{3\pi y}{b}+\\&-\frac{9f_{12}}{(1+16\lambda^2)^2}\cos\frac{4\pi y}{b}\Bigg]\cos\frac{\pi x}{a}+\lambda^4\Bigg[\frac{f_{11}^2+4f_{12}^2}{8}+\frac{9f_{11}f_{12}}{(4+\lambda^2)^2}\cos\frac{\pi y}{b}+\\&-\frac{f_{11}f_{12}}{(4+9\lambda^2)^2}\cos\frac{3\pi y}{b}\Bigg]\cos\frac{2\pi x}{a}+4\lambda^4 f_{22}^2\Bigg[\frac{f_{12}f_{22}}{9}+\frac{4f_{11}}{(9+\lambda^2)^2}\cos\frac{\pi y}{b}+\\&-\frac{f_{12}}{(9+16\lambda^2)^2}\cos\frac{4\pi y}{b}\Bigg]\cos\frac{3\pi x}{a}+\frac{\lambda^2}{32}\Bigg\}-\frac{\sigma_0 y^2}{2}\left(1-\frac{2}{3}\frac{y}{b}\right)-\tau_0 xy.\end{aligned} \tag{3.2}$$

where, $\lambda=a/b$. The last two terms of the above stress function $\Phi(x, y)$ constitute the solution of a homogeneous biharmonic equation. They fulfil the conditions of disk loading in a pre-critical state, i.e. when the coefficients $f_{11}=f_{22}=f_{12}=0$. The assumed conditions of rectilinearity of the disk edges are also satisfied. The analytical concept of these conditions consists in determining mutual transition of the edges, parallel in the initial state. The relative displacements of the disk edges, parallel to the axes y and x and determined by the formulae [4]

$$
\begin{aligned}
e_x &= -\frac{1}{E}\int_0^a \left[\frac{\partial^2 \Phi}{\partial y^2} - \nu\frac{\partial^2 \Phi}{\partial x^2} - \frac{E}{2}\left(\frac{\partial w}{\partial x}\right)^2\right] dx, \\
e_y &= -\frac{1}{E}\int_0^b \left[\frac{\partial^2 \Phi}{\partial x^2} - \nu\frac{\partial^2 \Phi}{\partial y^2} - \frac{E}{2}\left(\frac{\partial w}{\partial y}\right)^2\right] dy,
\end{aligned} \tag{3.3}
$$

are, respectively, a linear function of the coordinate y, for the edges $x=0$ and $x=a$, constant value for the edges $y=0$ and $y=b$; it results from the following expressions

$$
\begin{aligned}
e_x &= -\frac{\sigma_0}{E}a\left(1-2\frac{y}{b}\right) - \frac{\pi^2}{8a}(f_{11}^2+4f_{22}^2+f_{12}^2), \\
e_y &= -\frac{\pi^2}{8b}(f_{11}^2+4f_{22}^2+4f_{12}^2).
\end{aligned} \tag{3.4}
$$

In order to determine the unknown coefficients f_{11}, f_{22} and f_{12} appearing in the assumed deflection function $w(x, y)$ and also in the determined stress function $\Phi(x, y)$, the Kármán equation (2.2) has been made use of. This equation was solved by employing the Bubnov-Galerkin's method. Thus, in the case considered the following system of equations is used:

$$
\begin{aligned}
&\int_0^a\int_0^b X(w, \Phi)\sin\frac{\pi x}{a}\sin\frac{\pi y}{b}\,dx\,dy=0, \\
&\int_0^a\int_0^b X(w, \Phi)\sin\frac{2\pi X}{a}\sin\frac{2\pi y}{b}\,dx\,dy=0, \\
&\int_0^a\int_0^b X(w, \Phi)\sin\frac{\pi x}{a}\sin\frac{2\pi y}{b}\,dx\,dy=0,
\end{aligned} \tag{3.5}
$$

where, by the symbol $X(w, \Phi)$, the left side of Eq. (2.2) is denoted. For further considerations the following dimensionless coefficients are introduced:

the deflection coefficients

$$
\xi_{11}=\frac{f_{11}}{h}, \quad \xi_{22}=\frac{f_{22}}{h}, \quad \xi_{12}=\frac{f_{12}}{h}, \tag{3.6}
$$

and the disk loading coefficients

$$s=\frac{\sigma_0}{E}\left(\frac{a}{h}\right)^2, \qquad t=\frac{\tau_0}{E}\left(\frac{a}{h}\right)^2. \tag{3.7}$$

Then, after integrating, Eqs. (3.5) are reduced to the following system of three nonlinear, homogeneous, algebraic equations:

$$\frac{\left(\frac{1}{\lambda}+\lambda\right)^2}{48\,(1-\nu^2)}\xi_{11}-\frac{32}{9\pi^4\lambda}\xi_{22}\,t-\frac{8}{9\pi^4\lambda^2}\xi_{12}\,s+\frac{1+\lambda^4}{64\lambda^2}\xi_{11}^3+ \tag{3.8}$$

$$+\frac{\lambda^2}{64}\left[8+\frac{81}{(4+\lambda^2)^2}+\frac{1}{(4+9\lambda^2)^2}\right]\xi_{11}\,\xi_{12}^2+4\lambda^2\left[\frac{1}{(1+9\lambda^2)^2}+\frac{1}{(9+\lambda^2)^2}\right]\xi_{11}\,\xi_{22}^2=0;$$

$$-\frac{32}{9\pi^4\lambda}\xi_{11}\,t+\frac{\left(\frac{1}{\lambda}+\lambda\right)^2}{3\,(1-\nu^2)}\xi_{22}+\frac{1+\lambda^4}{4\lambda^2}\xi_{22}^3+\frac{\lambda^2}{4}\left[\frac{1+16\lambda^4}{4\lambda^4}+\frac{81}{(1+16\lambda^2)^2}+\right. \tag{3.9}$$

$$\left.+\frac{1}{(9+16\lambda^2)^2}\right]\xi_{22}\,\xi_{12}^2+4\lambda^2\left[\frac{1}{(1+9\lambda^2)^2}+\frac{1}{(9+\lambda^2)^2}\right]\xi_{22}\,\xi_{11}^2=0;$$

$$-\frac{8}{9\pi^4\lambda^2}\xi_{11}\,s+\frac{\left(\frac{1}{\lambda}+4\lambda\right)^2}{48\,(1-\nu^2)}\xi_{12}+\frac{1+16\lambda^4}{64\lambda^2}\xi_{12}^3+ \tag{3.10}$$

$$+\frac{\lambda^2}{64}\left[4\,(1+\lambda^4)+\frac{81}{(4+\lambda^2)^2}+\frac{1}{(4+9\lambda^2)^2}\right]\xi_{11}^2\,\xi_{12}+$$

$$+\frac{\lambda^2}{4}\left[\frac{1+16\lambda^4}{4\lambda^4}+\frac{81}{(1+16\lambda^2)^2}+\frac{1}{(9+16\lambda^2)^2}\right]\xi_{12}\,\xi_{22}^2=0.$$

These equations contains contain five unknown values, namely the coefficients ξ_{11}, ξ_{22}, ξ_{12}, s and t.

To determine the critical values of the dimensionless disk loading coefficients s and t, the same system of equations (3.8)–(3.10) may be utilized. These critical values are determined from the condition that the principal determinant of the linear part of the equation system be equal to zero.

$$W=\begin{vmatrix} \dfrac{\left(\frac{1}{\lambda}+\lambda\right)^2}{48\,(1-\nu^2)} & \dfrac{32}{9\pi^4\lambda}t & \dfrac{8}{9\pi^4\lambda^2}s \\ -\dfrac{32}{9\pi^4\lambda}t & \dfrac{\left(\frac{1}{\lambda}+\lambda\right)^2}{3\,(1-\nu^2)} & 0 \\ -\dfrac{8s}{9\pi^4\lambda^2} & 0 & \dfrac{\left(\frac{1}{\lambda}+4\lambda\right)^2}{48\,(1-\nu^2)} \end{vmatrix}=0. \tag{3.11}$$

After this determinant has been expanded, the following relation for determining the critical values of the disk loading coefficients t and s is obtained:

$$s^2 = \frac{9\pi^8 (1+\lambda^2)^2 (1+4\lambda^2)^2}{256 \cdot 64 (1-\nu^2)^2} - \lambda^2 \left(\frac{1+4\lambda^2}{1+\lambda^2} \right)^2 t^2. \tag{3.12}$$

On the basis of the above formula, the diagrams of the relation $t=t(s)$, for different values of the disk form coefficient λ, have been made up (Fig. 2). The value of the Poisson's ratio has been assumed to be $\nu=0.3$.

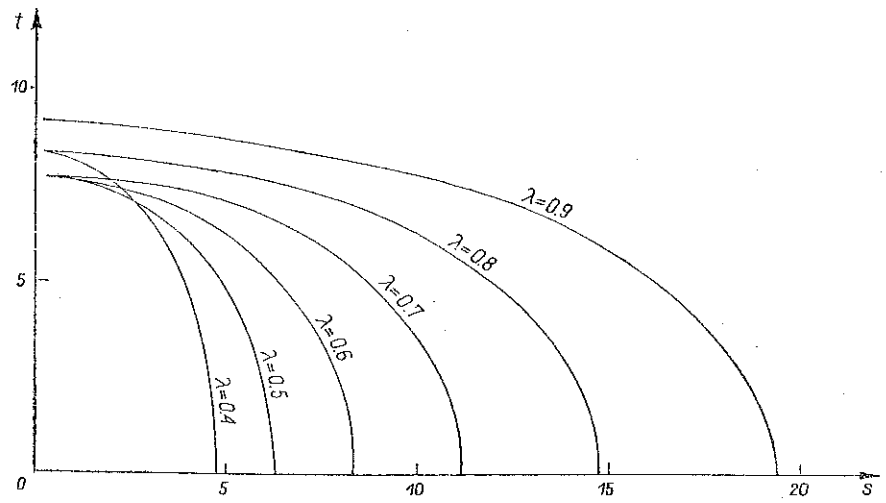

FIG. 2. Curves of critical states of the disk for different values of the disk form coefficient (for $\nu=0.3$)

The critical values of disk loading in limiting of the disk under pure bending ($t=0$) or pure shear ($s=0$), determined from the curves and presented in Fig. 2 have been compared with the literature data given in [3, 7, 8]. These values are practically equal to accurate critical values given in the literature; the maximum error is smaller than 3% for the accepted range of the coefficient λ.

The dimensionless coefficients t and s of disk loading for the post-buckling state, i.e. when the coefficients $\xi_{11} \neq 0$, $\xi_{22} \neq 0$ and $\xi_{12} \neq 0$, were determined by the following formulae resulting from Eqs. (3.9) and (3.10):

$$t = \frac{9\pi^4 \lambda}{32} \left\{ \frac{\left(\frac{1}{\lambda} + \lambda \right)^2}{3(1-\nu^2)} \frac{\xi_{22}}{\xi_{11}} + \frac{1+\lambda^4}{4\lambda^2} \frac{\xi_{22}^2}{\xi_{11}} + \frac{\lambda^2}{4} \left[\frac{1+16\lambda^4}{4\lambda^2} + \frac{81}{(1+16\lambda^2)^2} + \right. \right. \tag{3.13}$$

$$\left. \left. + \frac{1}{(9+16\lambda^2)^2} \right] \frac{\xi_{22} \xi_{12}^2}{\xi_{11}} + 4\lambda^2 \left[\frac{1}{(1+9\lambda^2)^2} + \frac{1}{(9+\lambda^2)^2} \right] \xi_{11} \xi_{22} \right.$$

and

$$(3.14)\quad s=\frac{9\pi^4\lambda^2}{32}\left\{\frac{\left(\frac{1}{\lambda}+4\lambda\right)^2}{12(1-\nu^2)}\frac{\xi_{12}}{\xi_{11}}+\frac{1+16\lambda^4}{16\lambda^2}\frac{\xi_{12}^3}{\xi_{11}}+\frac{\lambda^2}{16}\left[4(1+\lambda^4)+\frac{81}{(4+\lambda^2)^2}+\right.\right.$$
$$\left.\left.+\frac{1}{(4+9\lambda^2)^2}\right]\xi_{11}\xi_{22}+\lambda^2\left[\frac{1+16\lambda^4}{4\lambda^4}+\frac{81}{(1+16\lambda^2)^2}+\frac{1}{(9+16\lambda^2)^2}\right]\frac{\xi_{12}\xi_{22}^2}{\xi_{11}}\right\}.$$

To determine the unknown coefficients ξ_{11}, ξ_{22} and ξ_{12} of a disk deflection for the post-buckling state, Eq. (3.8) was utilized. This equation, after eliminating the dimensionless coefficients t and s by means of the expressions (3.13) and (3.14), has the following form:

$$(3.15)\quad \frac{1+16\lambda^4}{64\lambda^2}\frac{\xi_{12}^4}{\xi_{11}}+\left\{\frac{\left(\frac{1}{\lambda}+4\lambda\right)^2}{48(1-\nu^2)}\frac{1}{\xi_{11}}+\frac{1-\lambda^4}{16\lambda^2}\xi_{11}+\right.$$
$$\left.+\frac{\lambda^2}{2}\left[\frac{1+16\lambda^4}{4\lambda^4}+\frac{81}{(1+16\lambda^2)^2}+\frac{1}{(9+16\lambda^2)^2}\right]\frac{\xi_{22}^2}{\xi_{11}}\right\}\xi_{12}^2+$$
$$+\frac{\left(\frac{1}{\lambda}+\lambda\right)^2}{48(1-\nu)^2}\left(\frac{16\xi_{22}^2-\xi_{11}^2}{\xi_{11}}\right)+\frac{1+\lambda^4}{64\lambda^2}\left(\frac{16\xi_{22}^4-\xi_{11}^4}{\xi_{11}}\right)=0.$$

To solve the equation above, the successive pairs of the dimensionless coefficients ξ_{11} and ξ_{22} were assumed. Then Eq. (3.15) becomes for each of these pairs a biquadratic equation for the unknown coefficient ξ_{12}. The solution of this equation consists of two real roots with equal absolute values, but opposite signs. In further computations a positive value of the coefficient ξ_{12} was taken. Then, the values of the disk deflection coefficients ξ_{11}, ξ_{22} and ξ_{12}, being known, it is possible to determine from Eqs. (3.13) and (3.14) the values of the disk loading coefficients s and t and, next, the components of stress and strain of the disk considered.

After stability loss the state of stress is represented by the superposition of two states, namely: 1) the membrane state with the components σ_x, σ_y and τ_{xy}, constant across thickness, and 2) the bending state in which the components σ_{xg}, σ_{yg} and τ_g change linearly across the disk thickness, assuming maximal values at two outside surfaces, and vanishing at the middle surface of the disk.

The shear stresses τ_{xz} and τ_{yz} are disregarded as small. In further considerations, dimensionless stresses are introduced:

for the membrane stress state:

$$(3.16)\quad \sigma_x^*=\frac{\sigma_x}{E}\left(\frac{a}{h}\right)^2,\quad \sigma_y^*=\frac{\sigma_y}{E}\left(\frac{a}{h}\right)^2,\quad \tau_{xy}^*=\frac{\tau_{xy}}{E}\left(\frac{a}{h}\right)^2,$$

for the bending stress state:

$$(3.17)\quad \sigma_{xg}^{*}=\frac{(\sigma_{xg})_{z=+\frac{h}{2}}}{E}\left(\frac{a}{h}\right)^2,\qquad \sigma_{yg}^{*}=\frac{(\sigma_{yg})_{z=+\frac{h}{2}}}{E}\left(\frac{a}{h}\right)^2,\qquad \tau_{g}^{*}=\frac{(\tau_{g})_{z=+\frac{h}{2}}}{E}\left(\frac{a}{h}\right)^2,$$

where

$$(3.18)\quad \begin{aligned}(\sigma_{xy})_{z=+\frac{h}{2}}&=\frac{6M_x}{h^2}=\frac{Eh}{2(1-\nu^2)}\left(\frac{\partial^2 w}{\partial x^2}+\nu\frac{\partial^2 w}{\partial y^2}\right),\\ (\sigma_{yg})_{z=+\frac{h}{2}}&=\frac{6M_x}{h^2}=\frac{Eh}{2(1-\nu^2)}\left(\frac{\partial^2 w}{\partial y^2}+\nu\frac{\partial^2 w}{\partial x^2}\right),\\ (\tau_{g})_{z=+\frac{h}{2}}&=\frac{6M_{xy}}{h^2}=\frac{Eh}{2(1+\nu)}\frac{\partial^2 w}{\partial x\,\partial y},\end{aligned}$$

M_x, M_y, M_{xy} are the sectional moments referred to the unit length of the cross-section element, cut from the disk.

In the considered case, the dimensionless components σ_x^{*}, σ_y^{*} and τ_{xy}^{*} mentioned above of the membrane stresses and σ_{xg}^{*}, σ_{yg}^{*} and τ_{g}^{*} of the bending stresses state are expressed by the following formulae:

$$\begin{aligned}(3.19)\quad \sigma_x^{*}=\frac{1}{E}\left(\frac{a}{h}\right)^2\frac{\partial^2\Phi}{\partial y^2}=-\frac{\pi^2}{4}\Bigg\{&\xi_{11}\xi_{12}\cos\frac{\pi y}{b}+\frac{1}{2}\xi_{11}^2\cos\frac{2\pi y}{b}+\\ &+\xi_{11}\xi_{12}\cos\frac{3\pi y}{b}+\frac{1}{2}(\xi_{12}^2+\xi_{22}^2)\cos\frac{4\pi y}{b}+9\lambda^4\Bigg[\frac{16}{(1+9\lambda^2)^2}\xi_{11}\xi_{22}\cos\frac{3\pi y}{b}+\\ &+\frac{63}{(1+16\lambda^2)^2}\xi_{22}\xi_{12}\cos\frac{4\pi y}{b}\Bigg]\cos\frac{\pi x}{a}+9\lambda^4\xi_{11}\xi_{12}\Bigg[\frac{1}{(4+\lambda^2)^2}\cos\frac{\pi y}{b}-\\ &-\frac{1}{(4+9\lambda^2)^2}\cos\frac{3\pi y}{b}\Bigg]\cos\frac{2\pi x}{a}+16\lambda^4\Bigg[\frac{1}{(9+\lambda^2)^2}\xi_{11}\xi_{22}\cos\frac{\pi y}{b}-\\ &-\frac{4}{(9+16\lambda^2)^2}\xi_{22}\xi_{12}\cos\frac{4\pi y}{b}\Bigg]\cos\frac{3\pi x}{a}\Bigg\}-s\left(1-2\frac{y}{b}\right);\end{aligned}$$

$$\begin{aligned}(3.20)\quad \sigma_y^{*}=\frac{1}{E}\left(\frac{a}{h}\right)^2\frac{\partial^2\Phi}{\partial x^2}=-\frac{\pi^2\lambda^2}{4}\Bigg\{&-4\xi_{22}\xi_{12}\cos\frac{\pi x}{a}+\\ &+\frac{1}{2}(\xi_{11}^2+4\xi_{12}^2)\cos\frac{2\pi x}{a}+4\xi_{22}\xi_{12}\cos\frac{3\pi x}{a}+2\xi_{22}^2\cos\frac{4\pi x}{a}+\\ &+36\Bigg[\frac{\xi_{11}\xi_{12}}{(4+\lambda^2)^2}\cos\frac{2\pi x}{a}+\frac{4\xi_{11}\xi_{22}}{(9+\lambda^2)^2}\cos\frac{3\pi x}{a}\Bigg]\cos\frac{\pi y}{b}+4\Bigg[\frac{4\xi_{11}\xi_{22}}{(1+9\lambda^2)^2}\cos\frac{\pi x}{a}-\\ &-\frac{\xi_{11}\xi_{12}}{(4+9\lambda^2)^2}\cos\frac{2\pi x}{a}\Bigg]\cos\frac{3\pi y}{b}+36\xi_{22}\xi_{12}\Bigg[\frac{1}{(1+16\lambda^2)^2}\cos\frac{\pi x}{a}-\\ &-\frac{1}{(9+16\lambda^2)^2}\cos\frac{3\pi x}{a}\Bigg]\cos\frac{4\pi y}{b}\Bigg\};\end{aligned}$$

$$(3.21)\quad \tau_{xy}^{*}=-\frac{1}{E}\left(\frac{a}{h}\right)^{2}\frac{\partial^{2}\Phi}{\partial x\,\partial y}=-\frac{3\pi^{2}\lambda^{3}}{2}\left\{\left[\frac{3\xi_{11}\xi_{12}}{(4+\lambda^{2})^{2}}\sin\frac{2\pi x}{a}+\right.\right.$$

$$+\left.\frac{8\xi_{11}\xi_{22}}{(9+\lambda^{2})^{2}}\sin\frac{3\pi x}{a}\right]\sin\frac{\pi y}{b}+\left[\frac{8\xi_{11}\xi_{22}}{(1+9\lambda^{2})^{2}}\sin\frac{\pi x}{a}-\frac{\xi_{11}\xi_{22}}{(4+9\lambda^{2})^{2}}\sin\frac{2\pi x}{a}\right]\sin\frac{3\pi y}{b}+$$

$$\left.+8\xi_{22}\xi_{12}\left[\frac{3}{(1+16\lambda^{2})^{2}}\sin\frac{\pi x}{a}-\frac{1}{(9+16\lambda^{2})^{2}}\sin\frac{3\pi x}{a}\right]\sin\frac{4\pi y}{b}\right\}+t$$

and

$$(3.22)\quad \sigma_{xg}^{*}=\frac{\pi^{2}}{2(1-\nu^{2})}\left[(1+\nu\lambda^{2})\xi_{11}\sin\frac{\pi x}{a}\sin\frac{\pi y}{b}+\right.$$

$$\left.+4(1+\nu\lambda^{2})\xi_{22}\sin\frac{2\pi x}{a}\sin\frac{2\pi y}{b}+(1+4\nu\lambda^{2})\xi_{12}\sin\frac{\pi x}{a}\sin\frac{2\pi y}{b}\right],$$

$$(3.23)\quad \sigma_{yg}^{*}=\frac{\pi^{2}}{2(1-\nu^{2})}\left[(\lambda^{2}+\nu)\xi_{11}\sin\frac{\pi x}{a}\sin\frac{\pi y}{b}+\right.$$

$$\left.+4(\lambda^{2}+\nu)\xi_{22}\sin\frac{2\pi x}{a}\sin\frac{2\pi y}{b}+(4\lambda^{2}+\nu)\xi_{12}\sin\frac{\pi x}{a}\sin\frac{2\pi y}{b}\right],$$

$$(3.24)\quad \tau_{g}^{*}=\frac{\pi^{2}\lambda}{2(1+\nu)}\left[\xi_{11}\cos\frac{\pi x}{a}\cos\frac{\pi y}{b}+\right.$$

$$\left.+4\xi_{12}\cos\frac{2\pi x}{a}\cos\frac{2\pi y}{b}+2\xi_{12}\cos\frac{\pi x}{a}\cos\frac{2\pi y}{b}\right].$$

On the basis of the formulae (3.19)–(3.24), the reduced stresses have also been determined according to the Huber-Mises hypothesis. The maximal values of these stresses appear on the upper ($z=-h/2$) or on the lower ($z=h/2$) surface of the disk. Introducing the dimensionless coefficient of these stresses

$$(3.25)\quad \sigma_{\mathrm{red}}^{*}=\frac{\sigma_{\mathrm{red}}}{E}\left(\frac{a}{h}\right)^{2},$$

the dimensionless reduced stress in any point of the upper or lower surface of the disk is expressed as follows:

$$(3.26)\quad \sigma_{\mathrm{red}}^{*}(x,y)=[\sigma_{x}^{*}\pm\sigma_{xg}^{*})^{2}+(\sigma_{y}^{*}\pm\sigma_{yg}^{*})^{2}-(\sigma_{x}^{*}\pm\sigma_{xg}^{*})(\sigma_{y}^{*}\pm\sigma_{yg}^{*})+3(\tau_{xy}^{*}+\tau_{g}^{*})^{2}].^{1/2}.$$

The signs "plus" (+) in this formula refer to points of the lower disk surface ($z=+h/2$), whereas the signs "minus" (−) to points of the upper surface ($z=-h/2$).

The deflection of the disk in the post-buckling state have also been determined by means of the dimensionless coefficient

$$(3.27)\quad w^{*}=\frac{w}{h}.$$

The computations which were to determine the maximal values of the dimensionless reduced stress coefficient $(\sigma^*_{red})_{max}$ were performed in the following manner: a hundred uniformly distributed points were chosen on the disk middle surface and for each of them, for assumed values of the coefficients s and t, two values of the coefficients $(\sigma^*_{red})_{max}$ were determined according to the formula (3.26): one for the upper surface and the other for the lower surface of the disk. Next, the greatest of the determined values, that is $(\sigma^*_{red})_{max}$ was chosen, the maximum of $(\sigma^*_{red})_{max}$ was found numerically with different combinations of the disk loading coefficients s and t.

4. Results of detailed computations for a disk with the form coefficient $\lambda=0.9$

A detailed analysis of the post-buckling state of a disk under unidirectional bending and simultaneous shear was carried out, as an example, in the case of which the form coefficient $\lambda=0.9$. Detailed computations were made on the computer ODRA-1204. The results of these computations are presented in the form

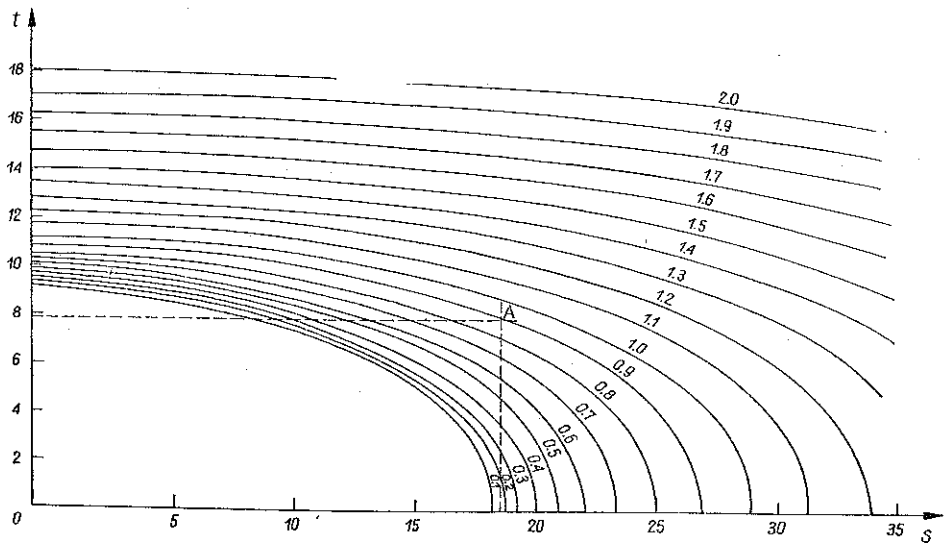

FIG. 3. Curves $\xi_{11}=$const of the dimensionless disk deflection coefficient for $\lambda=0.9$ and $\nu=0.3$.

of the diagrams shown in the successive figures. And thus, in Figs. 3, 4 and 5 are presented, successively, the curves $\xi_{11}=$const, $\xi_{22}=$const and $\xi_{12}=$const in the coordinates system $s-t$. Owing to this, if the values of the dimensionless disk loading coefficients s and t are known, the values of ξ_{11}, ξ_{22} and ξ_{12} can be easily read directly from the corresponding diagrams, or determined from these diagrams through interpolation.

A knowledge of the coefficients mentioned above then enables one to carry out an analysis of the disk deflections on the basis of the formula (3.27). In order to present more clearly the character of deflections in the post-buckling state of the

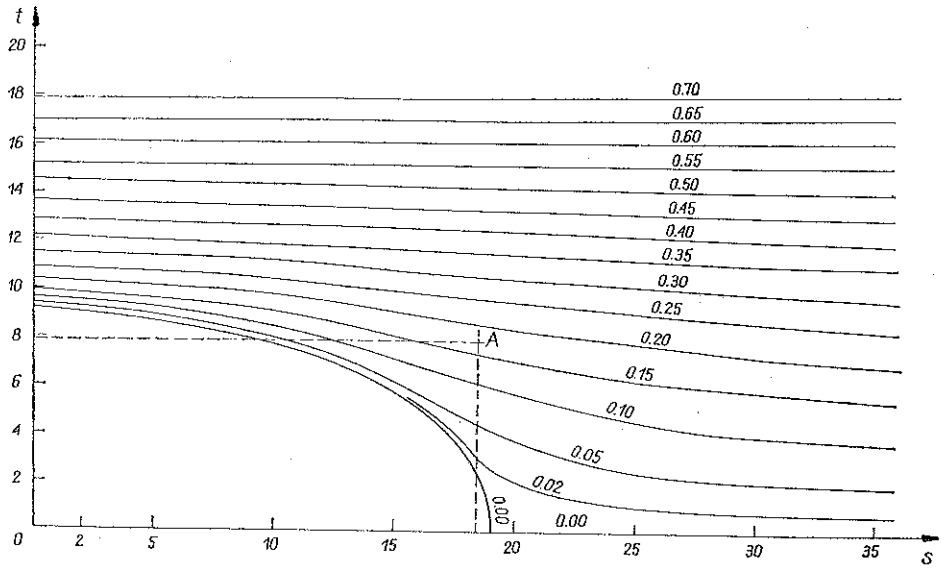

FIG. 4. Curves ξ_{22}=const of the dimensionless disk deflection coefficient for λ=0.9 and ν=0.3.

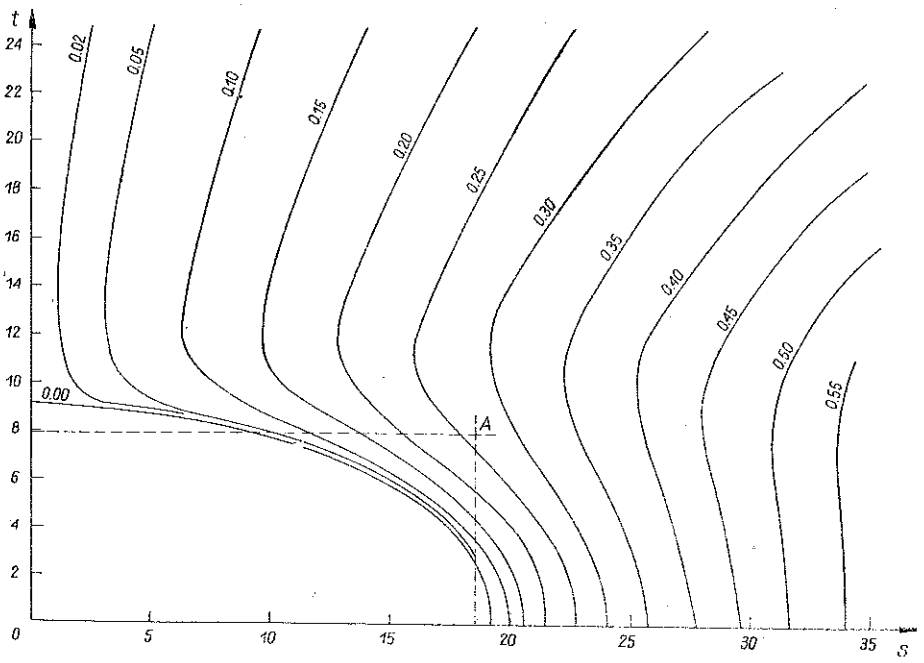

FIG. 5. Curves ξ_{22}=const of the dimensionless disk deflection coefficient for λ=0.9 and ν=0.3.

disk, the layer diagrams of deflections with different ratios of the loading coefficients were made up. These diagrams are presented in Fig. 6 by way of examples for the three following cases of the disk loading, namely: A — $s=25.95$ and $t=0$, i.e. in the case of pure bending, B — $s=22.98$ and $t=5.04$, C — $s=23.51$ and $t=11.33$, .ie. with considerable share of the shear loading,

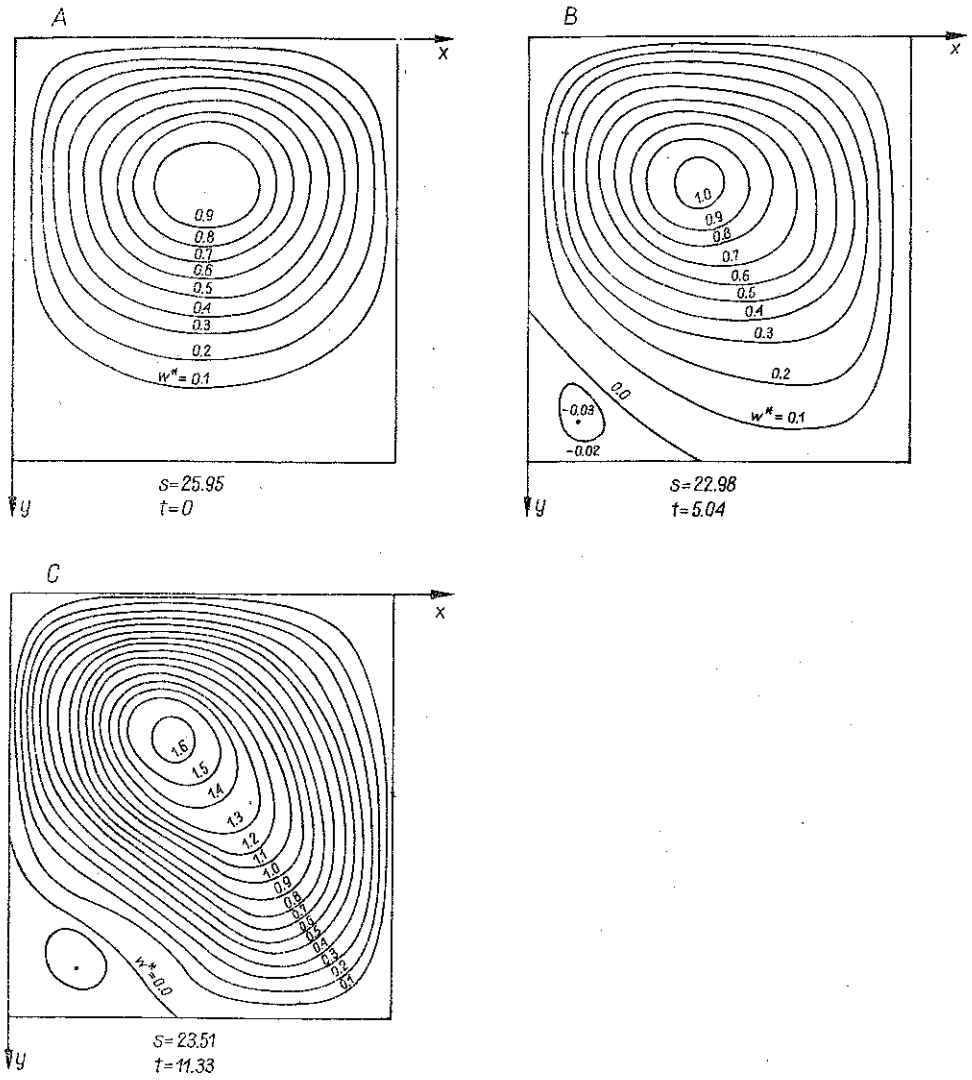

FIG. 6. Layer diagrams of disk deflections for different values of disk loading coefficients s and t for $\lambda=0.9$ and $\nu=0.3$.

Such a selection of the coefficient values s and t allows to estimate the influence of shear, combined with bending on the form of the deflected middle.

For the purpose of determing easily the maximal deflection w_{max}, the diagram presenting the curves $w^*_{max}=\text{const}$ in the coordinates $s-t$ was made up. This diagram

(Fig. 7) for the given values of the coefficients s and t makes it possible to determine directly the suitable value of the dimensionless coefficient w^*_{max} and, next, to calculate the real value of the maximal disk deflection on the basis of the definition (3.27). In order to determine maximum of the assumed deflection function $w(x, y)$, values of this function were computed in a hundred points uniformly distributed over the disk surface.

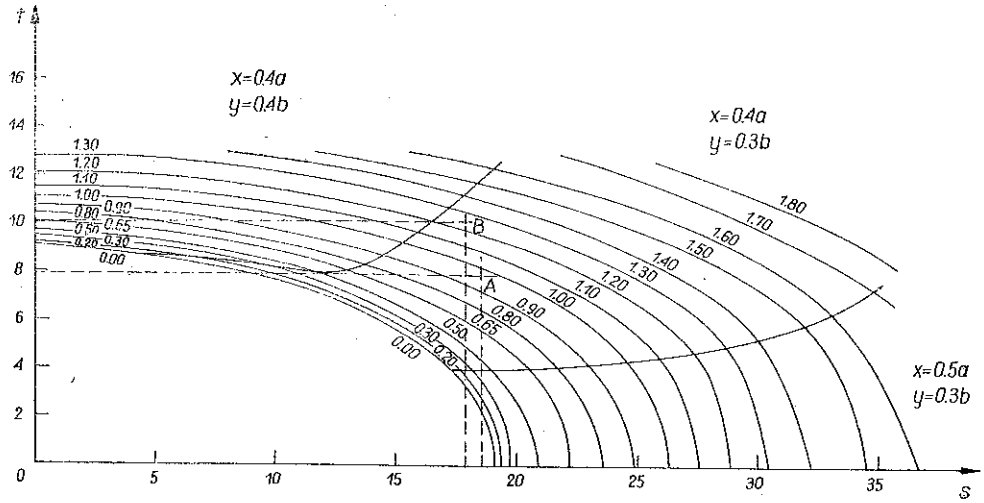

FIG. 7. Curves w^*_{max}=const of the dimensionless coefficient of the maximal disk deflection for λ=0.9 and ν=0.3.

From the computations it follows that the maximal deflections of the disk after stability loss may appear in the three different points of the middle surface, depending on the values of the loading coefficients s and t The coordinates of these points are: $x_{max}=0.4a$ and $y_{max}=0.4b$ — when the shear prevails in the loading of the disk, $x_{max}=0.4a$ and $y_{max}=0.3b$ — when the share of the shear in the loading of the disk is smaller than bending, $x_{max}=0.5a$ and $y_{max}=0.3b$ — when bending prevails.

In connection with this, the plane of the graph shown in Fig. 7 was divided into three areas. In each of these areas appear the same values of the coordinates x_{max} and y_{max} of the points of maximal disk deflection. The values of these coordinates were determined with the accuracy of $0.1a$ and $0.1b$.

For the case under discussion, i.e. when the disk form coefficient λ=0.9, the values of the reduced stress $(\sigma^*_{red})_{max}$ were also calculated by such means as the ones described in the previous section. On the basis of the results obtained, the next diagram was made up, presenting the curves $(\sigma^*_{red})_{max}$=const (Fig. 8) also in the coordinates system s- t.

In the course of computations the coordinates x_m and y_m of the point of the disk, revealing the maximum of the dimensionless reduced stress, were also determined. It turned out that the maximal reduced stresses appear at the points of the disk a) — $x_m=0.5a$ and $y_m=0$ — when the disk is under pure bending i. e. when $t=0$, b) — $x_m=0$ and $y_m=0$ — when the disk is under combined loading, i.e. when $s\neq0$ and $t\neq0$.

With regard to the accepted division of the disk, the coordinates x_m were determined with the accuracy of $0.1a$, and the coordinate y_m with the accuracy of $0.1b$.

If shear occurs in the loading of the disk, then, except for simultaneously applied bending, rapid displacement of the point takes place and this leads to the maximal values of the reduced stress. The point shifts from the middle of the disk (the point

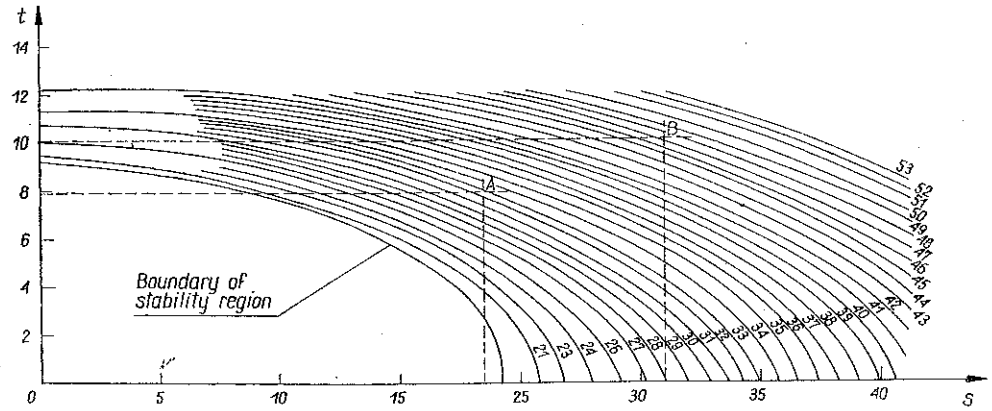

FIG. 8. Curves $(\sigma^*_{red})_{max}$=const of the dimensionless coefficient of the maximal reduced stresses for $\lambda=0.9$ and $\nu=0.3$.

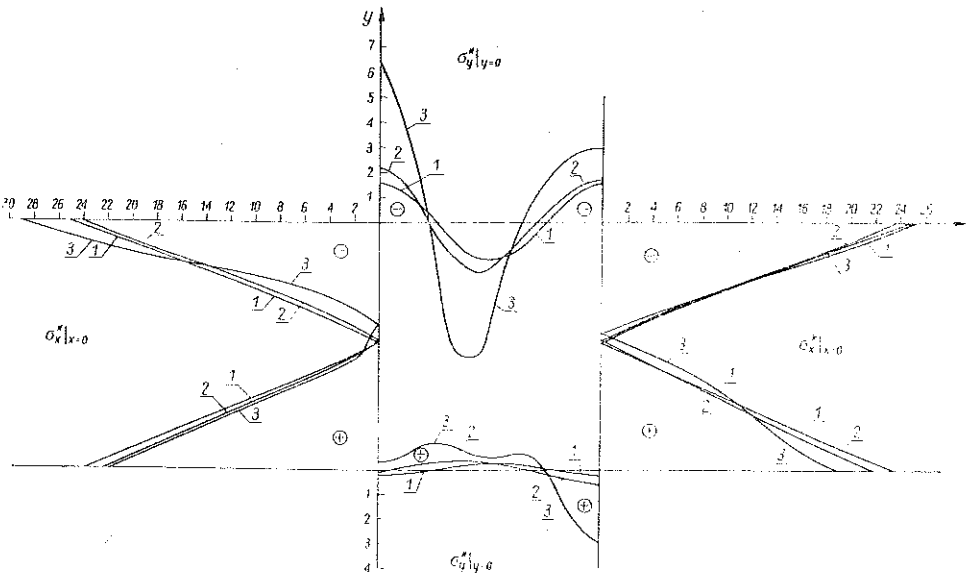

FIG. 9. Normal stresses at the disk edges after stability loss for $\lambda=0.9$ and $\nu=0.3$.

$x_m=0.5a$, $y_m=0$) to the corner ($x_m=0$ and $y_m=0$). Within the range of the performed computations with the accuracy assumed, it was impossible to determine in a continuous way the displacement of the point of maximum stress.

After stability loss, a change of stress distributions at the disk edges takes place. The stresses at the disk edges in the post-buckling state were determined on the

basis of the formulae (3.19), (3.20) and (3.21) for certain combinations of values of the loading coefficients s and t. The results of the computations are presented in the form of diagrams in Fig. 9.

From the stress distributions shown in this figure we see that: at the edges $y=0$ and $y=0$ loaded before stability loss only shear stresses τ_0, in the post-buckling state the normal self-equilibrated distributions appear; the distributions of the dimensionless stresses $(\sigma_y^*)_{y=0}$ and $(\sigma_y^*)_{y=b}$ are symmetrical to the axis $x=a/2$ when the disk is under pure disk bending only ($t=0$). If the disk is under unidirectional bending and simultaneous pure shear, the distributions of the stresses σ_y^* cease to be symmetrical to that axis.

The distributions of the dimensionless stresses σ_x^* along the edges $x=0$ and $x=a$ become nonlinear in the compressed part of the disk in the post-buckling state, and this nonlinearity increases with an increase of the values of the loading coefficients. The distributions of the dimensionless stresses σ_x^* in the post-buckling state of the disk are identical at both disk edges $x=0$ and $x=a$ when the disk is under pure bending only (i.e. when $t=0$). However, when $t\neq 0$, the distributions of the normal stresses σ_x^* on the edges $x=0$ and $x=a$ are different. These differences increase with an increase of the dimensionless coefficient t of the shear loading. The maximal values of the stresses σ_x^* appear at the two mentioned edges of the disk in the points $y=0$.

On all edges of the disk the components σ_{xg}^* and σ_{yg}^* due to bending are equal to zero. However, on these edges the shear component τ_g^* is not equal to zero.

5. Conclusions

All the relations describing the post-buckling state of the considered rectangular disk have been presented in the form of respective diagrams in the coordinates system (s, t) of the dimensionless loading coefficients. Owing to this, these diagrams can directly be made use of in practical calculations of the stability and post-buckling state of rectangular disks, like thin-walled structures. These diagrams yield information about the stress or strains in a disk subject to known external loadings. In the case when loadings exceeding the critical values may appear, such information is essential in estimating the load carrying capacity of a construction in conditions of local stability loss.

Moreover, these diagrams can be used for: determining admissible values of external loadings for a given disk, either on the basis of the maximal reduced stresses, strength criterion, or on the basis of the maximal deflection criterion, obtaining fundamental parameters of disk dimensions for some given external loading on the basis of the criterion mentioned above.

Formally, all the relations presented here being the approximate solution of the considered problem, are true for any value of a disk form coefficient λ. Practically, however, with the assumed form of the deflection function, according to the formula (3.1), the error will be small only for a disk whose shape is almost square, i.e. for orientation, when the disk form coefficient is $0.4\leqslant\lambda\leqslant 0.95$.

For a more thorough analysis of the problem, computations presented in this paper for the disk form coefficient $\lambda=0.9$ were also performed for some other values of the disk form coefficients λ, namely for $\lambda=0.4$, $\lambda=0.6$ and $\lambda=0.8$. In all these cases the character and the form of the fundamental curves, namely $\xi_{11}=\text{const}$, $\xi_{22}=\text{const}$, $\xi_{12}=\text{const}$, $w^*_{\max}=\text{const}$ or $(\sigma^*_{\text{red}})_{\max}=\text{const}$ presented also in the coordinates system $s-t$, were similar to the corresponding curves obtained for the case $\lambda=0.9$.

In order to obtain satisfactorily accurate results beyond the mentioned range of the disk form coefficients λ, i.e. when $\lambda>0.95$, one should assume the form of a deflection function $w(x, y)$ with a greater number of terms than that taken in the expression (3.1).

REFERENCES

1. Б. М. Броуде, *Устойчивость пластинок з элементах стальных конструкций*, Издат. Мин. строит. предпр. машиностроения, Москва 1949.
2. Ф. Блеих, *Устойчивость металлических конструкций*, (перевод с англ.), Госиздат. физ.-мат. лит., Москва 1959.
3. А. С. Вольмир, *Устойчивость деформируемых систем*, изд. 11-е, „Наука", Глав. ред. физ.-мат. лит., Москва 1937.
4. А. С. Вольмир, *Гибкие пластинки и оболочки*, Издат. техн. -теор. лит., Москва 1953.
5. И.И. Ааре, С. И. Индурм, *Закритическое поведение пластинок при сдвиге*, Труды Тал. политех. ин-та, Серия А, Нр 278, Таллин 1939.
6. И. И. Ааре, С. И. Индурм, *Исследование работы стенки тонкостенной металлической балки после потери устойчивости от сдвига и изгиба*, Труды Тал. политех. ин-та, Серия А, Нр 259, Таллин 1938.
7. W. Walczak, *Analiza stanu naprężenia tarczy prostokątnej po utracie stateczności, wywołanej zginaniem w płaszczyźnie tarczy* Arch. Budowy Maszyn, 12, 1, 1965.
8. S. P. Timoszenko, J. M. Gere, *Teoria stateczności sprężystej*, wyd. II, (tłum z ang.), Arkady, Warszawa 1963.

STRESZCZENIE

STATECZNOŚĆ I STAN ZAKRYTYCZNY PROSTOKĄTNEJ TARCZY PODDANEJ DZIAŁANIU JEDNOKIERUNKOWEGO ZGINANIA TARCZOWEGO I JEDNOCZESNEGO ŚCINANIA

Zagadnienie dotyczy izotopowej, prostokątnej tarczy, swobodnie podpartej wzdłuż obwodu. W celu otrzymania przybliżonego rozwiązania zagadnienia przyjęto funkcję ugięcia $w(x,y)$, opisującą kształt ugiętej powierzchni środkowej tarczy po jej utracie stateczności, w postaci szeregu, spełniającego warunki brzegowe zagadnienia. Wprowadzono także funkcję naprężeń Airy'ego $\Phi(x,y)$.

Dla określenia tych funkcji wykorzystano równania różniczkowe Kármána nieliniowej teorii płyt, a dla określenia nieznanych parametrów, występujących w funkcji ugięcia $w(x,y)$, zastosowano metodę Bubnowa-Galerkina.

W wyniku otrzymano wzory, na podstawie których określono składowe stanu naprężenia oraz odkształcenia tarczy za pomocą współczynników bezwymiarowych. Na podstawie tych wzorów przeprowadzono przykładowo szczegółowe obliczenia dla tarczy o stosunku długości boków $\lambda=a/b=0.9$. Wyniki tych obliczeń przedstawiono w postaci szeregu wykresów, opracowanych w sposób przydatny do obliczeń praktycznych.

Резюме

УСТОЙЧИВОСТЬ И ЗАКРИТИЧЕСКОЕ СОСТОЯНИЕ ПРЯМОУГОЛЬНОГО ДИСКА ПОДВЕРГНУТОГО ДЕЙСТВИЮ ОДНОНАПРАВЛЕННОГО ДИСКОВОГО ИЗГИБА И ИДНОВРЕМЕННОГО СДВИГА

Упомянутая в названии задача касается изотропного, прямоугольного диска свободно подпертого вдоль периметра. С целью получения приближенного решения задачи, функция прогиба $w(x, y)$ — описывающая форму прогиба срединной поверхности диска после потери устойчивости — принята в виде ряда, удовлетворяющего граничным условиям задачи. Введена также функция напрямений Эйри $\Phi(x, y)$.

Для определения этих функций использованы дифференциальные уравнения Кармана нелинейной теории плит, а для определения неизвестных параметров, выступающих в функции прогиба $w(x, y)$, применен метод Бубнова-Галеркина.

В результате получены формулы, на основе которых определены составляющие напряженного и деформационного состояни диска при помощи безразмерных коэффициентов. На основе этих формул проведены примерные подробные расчеты для диска с отношением длин сторон $\lambda = a/b = 0{,}9$. Результаты этих расчетов представлены в виде ряда графиков, изготовленых пригодным образом для практических расчетов.

TECHNICAL UNIVERSITY OF ŁÓDŹ
INSTITUTE OF APPLIED MECHANICS

Received December 9, 1978.